

EVOLUTION OF RECONNECTION ALONG AN ARCADE OF MAGNETIC LOOPS

PAOLO C. GRIGIS AND ARNOLD O. BENZ
Institute of Astronomy, ETH Zürich, 8092 Zürich, Switzerland
Draft version June 18, 2018

ABSTRACT

RHESSI observations of a solar flare showing continuous motions of double hard X-ray sources interpreted as footpoints of magnetic loops are presented. The temporal evolution shows many distinct emission peaks of duration of some tens of seconds ('elementary flare bursts'). Elementary flare bursts have been interpreted as instabilities or oscillations of the reconnection process leading to an unsteady release of magnetic energy. These interpretations based on two-dimensional concepts cannot explain these observations, showing that the flare elements are displaced in a third dimension along the arcade. Therefore, the observed flare elements are not a modulation of the reconnection process, but originate as this process progresses along an arcade of magnetic loops. Contrary to previous reports, we find no correlation between footpoint motion and hard X-ray flux. This flare apparently contradicts the predictions of the standard translation invariant 2.5D reconnection models.

Subject headings: Sun: flares — Sun: X-rays, gamma rays

1. INTRODUCTION

High-energetic electrons accelerated during solar flares emit bremsstrahlung hard X-rays (HXR), whose evolution in time can be followed in images, light curves, and spectra. This information is combined here to infer characteristics of the unknown acceleration process of these particles.

As for light curves, quasi-periodic modulations of the HXR flux on time scales of some tens of seconds (*Elementary Flare Bursts*; EFB) have long been known to observers (Parks & Winckler 1969; de Jager & de Jonge 1978). Spectral studies show that EFBs preferentially follow a characteristic *soft-hard-soft* spectral behavior (Grigis & Benz 2004, and references therein). The modulations of the HXR and microwave flux have been interpreted in 2D models of reconnection as fluctuations in the reconnection process due to global oscillations of the loop (Roberts et al. 1984; Nakariakov et al. 2003; Stepanov et al. 2004).

On the imaging front, early observational evidence from the *Solar Maximum Mission* Hard X-Ray Imaging Spectrometer (Hoyng et al. 1981) showed that HXR sources are found at the location of footpoints (FP) of magnetic loops. Different types of HXR sources located higher in the solar atmosphere were detected on some occasions: the *Yohkoh* Hard X-ray Telescope registered fainter *loop-top* sources above the soft X-ray loops (Masuda et al. 1994) and the *Reuven Ramaty High Energy Solar Spectrometric Imager* (RHESSI; Lin et al. 2002) observed *coronal* sources (Lin et al. 2003), as well as emission from collisionally thick coronal loops (Veronig & Brown 2004). However, the bulk of non-thermal HXRs comes from loop FPs.

Two FPs on opposite sides of a magnetic neutral line are expected in the standard model of eruptive flares (reviewed e.g. by Priest & Forbes 2002): The rapid eruption of a filament enables the magnetic field to reconnect, driving particle acceleration in lower loops. Electrons precipitating to a FP emit HXRs. In this scenario, one

expects the observed FP sources to drift apart as successive field lines are reconnected at higher altitudes. This explanation fits the long-known outward motion of H α ribbons parallel to the neutral line.

Reports on both the morphology and the time evolution of the FPs show a large range of behaviors: single (Takakura et al. 1983), double (Hoyng et al. 1981) and multiple sources are seen, and many authors observe FP motions of different kinds: decrease and increase in the FP separation across the neutral line; parallel and antiparallel movements along the arcade (for some recent observations see Fletcher & Hudson 2002; Liu et al. 2004; Qiu et al. 2004; Siarkowski & Falewicz 2004). This bewildering behavior demonstrates just how complex the flare phenomenon can be.

Krucker et al. (2003) presented high-resolution observations of a particularly interesting two-ribbon flare. One of the HXR FPs moved continuously along a ribbon, whereas the other two FPs showed no systematic motion. No motion perpendicular to the ribbons are noticeable, but the parallel motion correlated with the HXR flux. The observed behavior allowed Krucker et al. to interpret the observations still in terms of the standard reconnection model, where the motion is due to receding FPs. This requires a strongly sheared arcade and a not-specified complex magnetic structure including the 2 other FPs without systematic motion.

Here HXR source motions observed with RHESSI during a flare are reported that do not allow for such interpretation by the standard 2D reconnection model. We study also the relation between the spatial motion and the spectral evolution of EFBs in time.

2. OBSERVATIONS

RHESSI observed the Sun on November 9, 2002 from 12:23 to 13:28 UT, when it entered the shadow of the Earth, and it registered the HXR evolution of a solar flare of soft X-ray (GOES) importance M4.9. RHESSI was in a configuration well suited to the derivation of high-resolution HXR spectra and images: No decimation of the data was active during the flare and attenuation

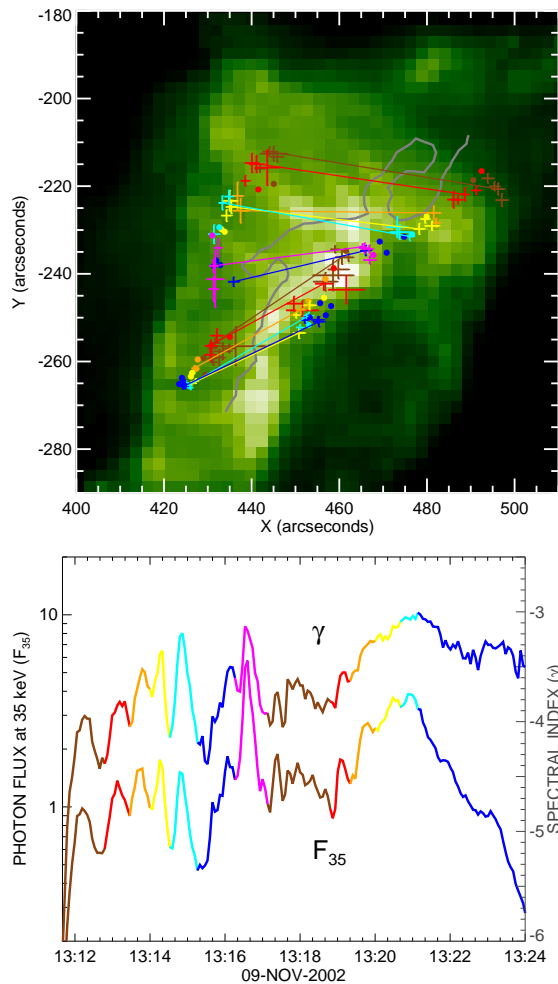


FIG. 1.— *Top*: SOHO/EIT 195 Å image of post-flare loops with the RHESSI HXR source positions superimposed. The positions of the 20 - 50 keV sources from the CLEAN images are represented by crosses with arm lengths proportional to the errors, positions from the PIXON images are given by circles. Simultaneous footpoints are connected and color coded according to the time intervals defined in the bottom part. The neutral line is shown in gray. *Bottom*: Time evolution of the flux and spectral index.

(Smith et al. 2002) was constantly in state 1 (thick attenuator in), thus ensuring that the detector dead time was below about 5% during the flare. Auxiliary data suggest that this flare was an eruptive event, displaying a post-flare loop arcade in the SOHO/EIT 195 Å images (Fig. 1), a moving Type IV radio burst (Phoenix spectrometer), and an associated fast CME (listed in the catalog by Yashiro et al. 2004).

Spatially integrated HXR spectra for this event were obtained at a cadence of one RHESSI rotation period (~ 4 s) and used in a previous study (Grigis & Benz 2004) to analyze the time evolution of the non-thermal part. Here we additionally produce HXR images averaged over two rotation periods (~ 8 s) in the energy band 20–50 keV using the CLEAN (Hurford et al. 2002) and the PIXON (Metcalf et al. 1996) reconstruction algorithms. The images resulting from the two different methods were inspected and compared. We discarded images of poor quality, obtaining 43 CLEAN and 69 PIXON images. Most images show two sources lo-

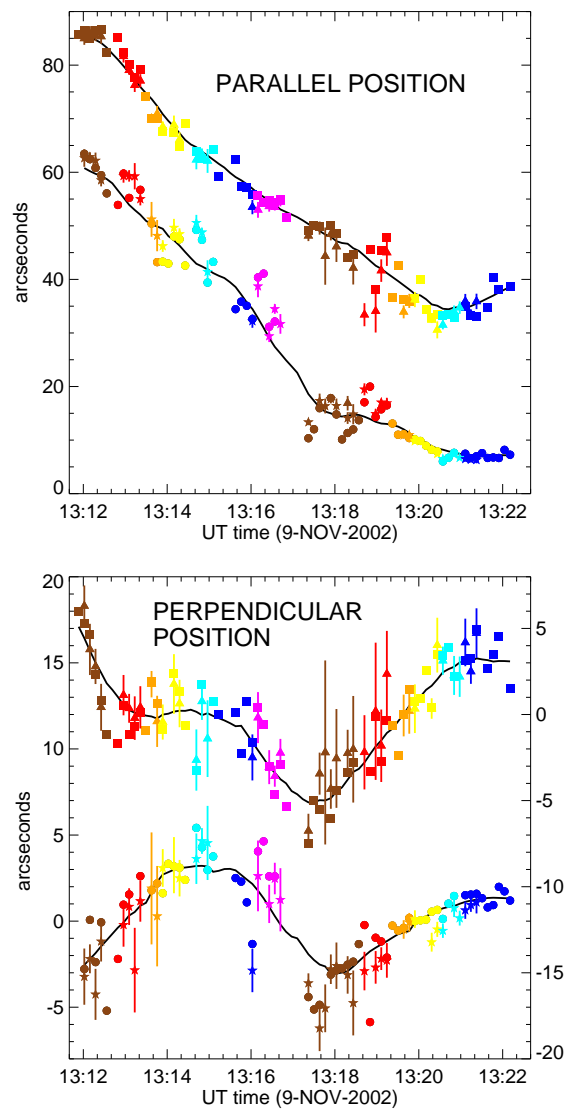


FIG. 2.— Time evolution of the source positions relative to the trend lines. The color code is the same as in Fig. 1, referring to the major subpeaks. Triangles and stars with error bars refer to values derived using CLEAN, squares and circles using PIXON, for the western and eastern FPs, respectively. *Top*: The upper curve displays the parallel coordinates of the western FPs, the lower curve the same of the eastern FPs. *Bottom*: Time evolution of the coordinate perpendicular to the regression lines. The upper curve refers to the western FP (scale on the right), the lower curve to the eastern FP (scale on the left). Both panels show in black the averaged smoothed motion for each FP (PIXON value), defining a new reference for detailed analysis.

cated at opposite sides of the magnetic neutral line, for some others only one source is clearly defined. We computed the source positions in each image by fitting a two-dimensional elliptical Gaussian to each visible source separately. For the CLEAN images we were able to estimate the statistical positional error by dividing the 1σ source width (provided by the Gaussian fit) by the signal to noise ratio (obtained dividing the peak flux by the standard deviation of the fluctuations in the image outside the sources). The average error estimated in this way amounts to $1.4''$. This method cannot be applied for the PIXON images, since the PIXON algorithm suppresses the noise in the image.

The evolution of the positions of the eastern and western FPs are shown in the top panel of Fig. 1 superimposed on a SOHO/EIT (Delaboudinière et al. 1995) image taken at 13:48 UT showing a post-flare loop arcade. The crosses represent the CLEAN positions with their error bars, and the circles the PIXON positions. We compensate for the effect of the solar rotation by rotating each source to the position it would assume at the time of the EIT image.

Both FPs start from the northern part of the image and move along the two ribbons visible to EIT in the south-east direction. The northern part of the arcade is wider than its southern end, and therefore the north-south movement along it effectively causes a convergence of the opposite FPs.

In the bottom panel of Fig. 1 the time evolution of the non-thermal HXR flux at 35 keV and the spectral index are presented. Emission peaks with a duration ranging from a few tens of seconds to the observational limit at 8 s can be noted, each showing soft-hard-soft behavior. The main peaks are drawn in a color different from their neighbors such that the source positions in the top panel, having the same code, can be followed in their temporal evolution.

To characterize the motion along the arcade, we define an eastern and a western regression line obtained by two independent least-squares fittings of all the positions of the eastern and western FPs. The two straight lines go from SE to NW and are not shown in Fig. 1. The lines are inclined by 74° (eastern) and 36° (western) to the E–W direction. From now on, every decomposition of a vector in its *parallel* and *perpendicular* components will refer to the directions given by the regression lines. The parallel coordinate increases from an arbitrary origin towards NW, whereas the perpendicular coordinate is positive in the direction which points away from the arcade.

The motions parallel and perpendicular to the two regression lines are presented in of Fig. 2. The FPs move predominantly along the lines, thus parallel to the ribbons. The parallel motion is quite smooth and continuous, especially for the western FP. For both FPs, the speed diminishes after about 13:17 UT. The only large discontinuity in the parallel motion is a possible $20''$ jump of the parallel eastern FP position after the strongest HXR peak when the eastern source is not detectable. Afterwards, the eastern FP move slower and get stationary after 13:20 UT. Contrary to previous reports, we find no correlation between FP speed and HXR flux.

Do subpeaks show motions perpendicularly outward from the ribbons as expected from the standard reconnection model? In Fig. 2 (bottom) this is not obvious, although the two FPs are apparently moving relative to the regression line. Note however, that the lines are converging, thus the effective FP separation decreases. Moreover, the ribbons are not straight. To study the question in more detail, we additionally define two smooth trend curves following the FP motions more closely. A moving average of the PIXON positions of each FP branch was computed, using a boxcar smoothing window of 15 elements, interpolating the missing points. The interval corresponds to a duration of 120 seconds, longer than all impulsive subpeaks in the HXR light curve (Fig. 1, bottom). The smooth trends are shown in Fig. 2 as black

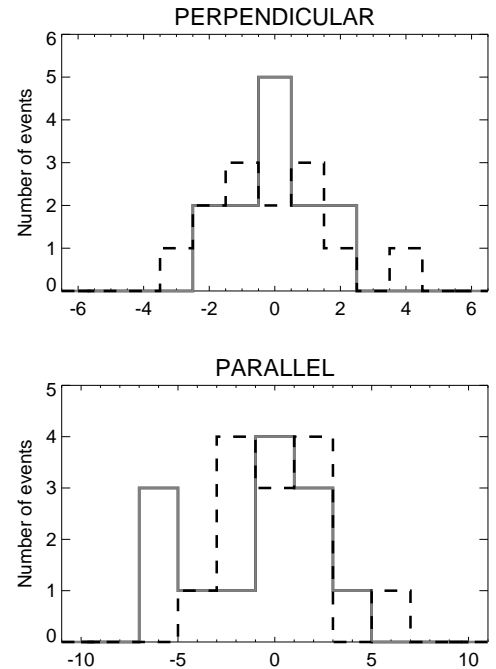


FIG. 3.— Distribution of the average motions during a peak in perpendicular and parallel directions relative to the time averaged trend curves. Eastern FPs are shown with continuous lines, western FPs with dashed lines.

continuous curves.

The standard reconnection model predicts outward FP motion at a given place in the arcade. In order to look for such systematic trends within HXR subpeaks, we took the parallel and perpendicular components of the difference vector from the smoothed source position to the observed PIXON positions. For each subpeak, we averaged the positions occurring during the first half and the second half, and calculated the difference second minus first half, Δ_{POS} , for both eastern and western sources.

For elementary flare bursts produced by standard reconnection, one would expect outward moving sources, thus Δ_{POS} being positive, at least on the average. Furthermore, the motion along the ribbons should be step-wise and discontinuous with Δ_{POS} being positive if each Elementary Flare Burst were a localized event. Figure 3 demonstrates that these expectations are not satisfied during subpeaks of this flare. The distribution of the average perpendicular motion during each peak shown in Fig. 3 has a mean $\Delta_{\text{POS}}^{\perp}$ value of $0.0'' \pm 0.4''$ for the eastern FP and $0.2'' \pm 0.5''$ for the western FP (the error is the standard error of the average). The mean value of the relative parallel motion during the peaks is $-1.0'' \pm 1.0''$ for the eastern FP and $0.4 \pm 0.7''$ for the western FP.

The global motion along the arcade progresses with an average velocity in the parallel direction of 63 km s^{-1} for the eastern FP and 55 km s^{-1} for the western FP. The lower velocity of the western FP is due to the fact that the latest data points have negative parallel velocities since they move backwards (Fig. 2). Averaging the absolute values of the parallel component of the velocity, we get 65 km s^{-1} for the western FP. A speed of about 110 km s^{-1} is maintained for 2 minutes in the western FP at the

beginning of the flare, while the data gap and possible jump around 13:17 in the eastern FP position requires 180 km s^{-1} .

The line connecting the two FPs is inclined with respect to the post-flare loops seen in the EIT image (Fig. 1). The angle is in the range of 25° to 70° , the post-flare loops being nearly perpendicular to the neutral line. This indicates that the HXR emitting loops are strongly sheared. RHESSI images at lower energy where thermal emission dominates the spectrum show sources or loops between the FPs. They appear to be coronal sources moving along the arcade with the FPs at higher energies.

3. CONCLUSION

We have analyzed RHESSI HXR observations of the time evolution of both images and spectra for a solar flare of GOES class M4.9. Surprisingly, the footpoints move smoothly along the two ribbons in contrast to the bursty evolution of the HXR flux. The observed Elementary Flare Bursts have durations between 30 s and less than 8 s, and show pronounced spectral soft-hard-soft behavior. The parallel source motions exclude the generally held notion of Elementary Flare Bursts being the modulation of a global reconnection process. Instead, the temporal modulation of the HXR flux and spectral index appear to be caused by a spatial displacement along the arcade. This could be caused by some disturbance propagating smoothly along the arcade, sequentially triggering a reconnection process in successive loops of the arcade. The disturbance would have to propagate with a speed in the range $50\text{--}150 \text{ km s}^{-1}$, much lower than the Alfvén velocity.

In the impulsive phase of this flare, magnetic energy release appears not in the form of a quasi-steady reconnection annihilating anti-parallel magnetic field and thus producing outward moving FPs. The main flare energy release at a given position in the arcade seems to last only a short time (order of a few seconds) and moves along the arcade in a systematic manner. The observed modulation of the HXR flux and the related anti-correlation of the spectral index in each Elementary Flare Burst appear to be caused by spatial variations of the acceleration efficiency. The temporal variations thus seem to be the result of a continuously moving trigger propagating through variable conditions in the arcade. The short lifetime of a FPs at a given position shows that particle trapping is not effective over timescales larger than several tens of seconds.

The observed simple and systematic motions set this event apart as a prototype for a type of HXR flare evolving *along the arcade*. The FP motions of this flare contradict clearly the expectations of the standard 2D reconnection model. The fact that we do not observe a systematic increase (up to the instrumental limits) of the separation of the FPs, does challenge the idea that the reconnection points move upwards and particles are accelerated in field lines successively farther out during the main HXR emitting phase of the flare. A possible interpretation is that the trigger releases the main energy stored in a two-dimensional loop structure within seconds, without noticeable FP motion, and moves on. Reconnection in the given structure may still continue, but with HXR emission below RHESSI sensitivity and at a much reduced energy release rate. Such secondary reconnection may be the cause of decimetric radio emissions continuing for 6 minutes after 13:22 UT, the end of HXR emission, and may produce the expansion of the two $\text{H}\alpha$ ribbons as observed in other flares.

We thus propose a scenario in which a disturbance, probably connected with the eruption of a filament, propagates along the arcade like a burning fuse, sequentially triggering reconnection and particle acceleration in the flare loops. The main HXR emission from the FP reflects the propagation of this disturbance, not the reconnection process at a given place in the arcade. If the dominating emission is strong and short-lived, the local conditions cause the observed temporal modulation.

The global evolution may be compatible with the standard model of an eruptive flare, if one allows the filament to erupt in such a way that one of its ends does not move while the other starts to rise. In this scenario the reconnection process spreads along the arcade until it reaches the end. The arcade erupts similar to the opening of a zipper, where the lower side run across the arcade and the upper side is the filament. Future studies of HXR FPs in a large number of flares may establish such a scenario and stimulate the development of 3D reconnection models needed to understand these observations.

The analysis of RHESSI data at ETH Zurich is partially supported by the Swiss National Science Foundation (grant nr. 200020-105366). We thank the many people who have contributed to the successful operation of RHESSI and acknowledge S. Krucker for helpful discussions.

REFERENCES

- Delaboudinière, J.-P., et al. 1995, *Sol. Phys.*, 162, 291
 de Jager, C., & de Jonge, G. 1978, *Sol. Phys.*, 58, 127
 Fletcher, L., & Hudson, H. S. 2002, *Sol. Phys.*, 210, 307
 Grigis, P. C., & Benz, A. O. 2004, *A&A*, 426, 1093
 Hoyng, P., et al. 1981, *ApJ*, 246, L155
 Hurford, G. J., et al. 2002, *Sol. Phys.*, 210, 61
 Krucker, S., Hurford, G. J., & Lin, R. P. 2003, *ApJ*, 595, L103
 Lin, R. P., et al. 2002, *Sol. Phys.*, 210, 3
 Lin, R. P., et al. 2003, *ApJ*, 595, L69
 Liu, W., Jiang, Y. W., Liu, S., & Petrosian, V. 2004, *ApJ*, 611, L53
 Masuda, S., Kosugi, T., Hara, H., Tsuneta, S., & Ogawara, Y. 1994, *Nature*, 371, 495
 Metcalf, T. R., Hudson, H. S., Kosugi, T., Puetter, R. C., & Pina, R. K. 1996, *ApJ*, 466, 585
 Nakariakov, V. M., Melnikov, V. F., & Reznikova, V. E. 2003, *A&A*, 412, L7
 Parks, G. K., & Winckler, J. R. 1969, *ApJ*, 155, L117
 Priest, E. R., & Forbes, T. G. 2002, *A&A Rev.*, 10, 313
 Qiu, J., Lee, J., & Gary, D. E. 2004, *ApJ*, 603, 335
 Roberts, B., Edwin, P. M., & Benz, A. O. 1984, *ApJ*, 279, 857
 Siarkowski, M., & Falewicz, R. 2004, *A&A*, 428, 219
 Smith, D. M., et al. 2002, *Sol. Phys.*, 210, 33
 Stepanov, A. V., et al. 2004, *Astronomy Letters*, 30, 480
 Takakura, T., Tsuneta, S., Nitta, N., & Ohki, K. 1983, *Sol. Phys.*, 86, 323
 Veronig, A. M., & Brown, J. C. 2004, *ApJ*, 603, L117
 Yashiro, S., Gopalswamy, N., Michalek, G., St. Cyr, O. C., Plunkett, S. P., Rich, N. B., & Howard, R. A. 2004, *Journal of Geophysical Research (Space Physics)*, 7105